Intermittent upwelling events trigger delayed, major, and reproducible pico-nanophytoplankton responses in coastal oligotrophic waters

R. Fuchs[1,2*], V. Rossi[2†], C. Caille[3‡], N. Bensoussan[2§], C. Pinazo[2¶], O. Grosso[2‖], M. Thyssen[2]**

[1]Aix Marseille Univ, CNRS, Centrale Marseille, I2M, Marseille, France
[2]Aix Marseille Univ, Université de Toulon, CNRS, IRD, MIO, Marseille, France
[3]Sorbonne Université, CNRS, LOMIC, Banyuls-sur-Mer, France

Key Points:

- Phytoplankton abundance (biomass, resp.) reactions start less than 2 days (4 days, resp.) after the upwelling onset and last 2 to 5 days.
- Except for *Synechococcus*, all group biomasses increase by 50-173% (up to +400%) during each event, then sharply decrease back to normal.
- Biomass peaks and daily rates of increase induced by the most extreme upwellings are of the same magnitude as the spring bloom ones.

*robin.fuchs@univ-amu.fr
†vincent.rossi@mio.osupytheas.fr
‡caillec@obs-banyuls.fr
§nathaniel.bensoussan@mio.osupytheas.fr
¶christel.pinazo@mio.osupytheas.fr
‖olivier.grosso@mio.osupytheas.fr
**melilotus.thyssen@mio.osupytheas.fr

Corresponding author: Melilotus Thyssen, `melilotus.thyssen@mio.osupytheas.fr`

Abstract

Pico-nanophytoplankton organisms are dominant in oligotrophic areas of the ocean but their highly adaptive growth rates make their contribution to the carbon cycle difficult to estimate. Here we address the response capacities of these microorganisms after intermittent wind gusts causing sporadic upwelling events in a coastal Mediterranean station. When the water column is stratified, corresponding to oligotrophic conditions, these events generate intense short-lived nutrient pulses and seawater temperature drops lasting six days on average and up to -10°C. Using a flow cytometer and statistical rupture-detection methods, we characterize the responses of five pico-nanophytoplankton functional groups at a two-hour frequency from September 2019 to November 2021. These events trigger delayed increases in both abundances and biomasses for most groups that can overpass spring bloom values, and are immediately followed by an overall decrease, suggesting a clear physical driver. Not considering these submesoscale events could significantly bias climate models and carbon budgets.

Plain Language Summary

Short-lived north-westerlies in the Mediterranean sea replace surface coastal waters with colder and richer in nutrients deeper waters from offshore. This phenomenon, called a sporadic upwelling event, lasts only a few days after the wind stops and induces brutal environmental shifts. During summer, upwellings generate drops in surface water temperature of up to 10°C and are expected to have a significant impact on phytoplankton cells. Small phytoplankton cells are conspicuous for their fast response to environmental changes thanks to their high division rates (up to several times a day). As a result, the biological response to wind-induced upwellings has to be studied using high-frequency measurements. Using four attributes for each of the five studied phytoplankton groups, we show that the number of cells of most groups rose strongly in less than two days after the temperature drop according to remarkable repeatable patterns. Similarly, their carbon content increased after less than four days. The reactions themselves lasted up to five days before going back near to the initial level. The described phytoplankton reactions to local upwelling events can be as important as the ones observed during the spring bloom, often regarded as the most important seasonal event for phytoplankton communities.

1 Introduction

Coastal zones play a significant role in the global carbon cycle as they sustain, despite large uncertainties, up to 30% of the global oceanic primary production (Gattuso et al., 1998). Previous research suggested the importance of taking into account the diversity and variability of near-shore ecosystems, which remain poorly known and under the influences of complex physical forcing (Borges et al., 2005; Bauer et al., 2013; Wimart-Rousseau et al., 2020) that strongly shapes phytoplankton communities (Morel & André, 1991; Antoine et al., 1995; Bosc et al., 2004; Armbrecht et al., 2014). Furthermore, there is evidence of the fast response capacities of phytoplankton after environmental changes, notably considering the prominence of meso and submesoscale processes in the ocean (Lévy et al., 2012). This is especially true for the pico-nanophytoplankton cells that present adaptive growth rates enhancing their competitive strategies (Lomas et al., 2009). The pico-nanophytoplankton size class is composed of polyphyletic unicellular photosynthetic microorganisms that dominate primary production in oligotrophic basins (Li, 1995; Grob et al., 2007) and are dominant in less oligotrophic conditions outside of the main spring and autumn bloom periods (Bolaños et al., 2020). They contribute substantially to the export of organic carbon into the deep layers mainly by aggregation or via grazing and subsequent sinking of organic materials (Richardson & Jackson, 2007; Lomas & Moran, 2011).

To assess the typical speed and frequency of community shifts that inform the capacity of pico-nanophytoplankton adaptation to abrupt changes in their environment, long-term and high-frequency sampling strategies allowing the separation of phytoplankton cells into functionally meaningful size classes are required. Martin-Platero et al. (2018) relied on a time series composed of daily samples for 93 days to show that physical forcing strongly shapes phytoplankton communities and that the observed patterns were highly dependent on the sampling frequency. Similarly, Martiny et al. (2016) have demonstrated positive significant correlations of cyanobacteria, pico and nanoeukaryotes abundances with temperature as well as nutrients using weekly samples over three years. Hunter-Cevera et al. (2020) used a 16-year long time series at an hourly frequency to highlight the seasonal cycles of *Synechococcus* abundances and proposed an explanation for *Synechococcus* blooms relying on growth rates variations. Wilkerson et al. (2006) demonstrated that wind-induced upwelling events followed by relaxation periods trigger optimal growth conditions for phytoplankton cells, depleting the upwelled nutrients and fostering a community of large phytoplanktonic cells (e.g. large diatoms), in line with Rossi et al. (2013). In more oligotrophic coastal areas, the responses of phytoplanktonic communities to short-lived enrichment events are more puzzling (Armbrecht et al., 2014) and suggest the prominence of small-sized phytoplanktonic cells. Thyssen et al. (2008) and Dugenne et al. (2014) have indeed shown important responses of pico-nanophytoplankton groups after strong north-westerlies events in the Bay of Marseille. Apart from atmospheric or riverine inputs and other classes of submesoscale frontal dynamics, sporadic wind-driven upwelling events are one major source of nutrients in the surface layers of various oligotrophic coastal areas (Millot, 1979; Bakun & Agostini, 2001; Palma & Matano, 2009; Rossi et al., 2014). While their hydrographic impacts, temperature cooling and nutrient enrichment of surface waters, are relatively well documented, little information exists on how they influence phytoplankton communities. The Bay of Marseille constitutes a natural laboratory to study the biological impacts of such events since they are common during stratified summer periods (Odic et al., 2022).

To our knowledge, all previous studies did not focus on wind events exclusively (Martiny et al., 2016; Hunter-Cevera et al., 2020), had low statistical power (Thyssen et al., 2008; Dugenne et al., 2014; Martin-Platero et al., 2018), had an insufficient temporal resolution (daily frequency for Wilkerson et al. (2006), weekly frequency in Martiny et al. (2016)) or did not fully resolve the pico-nanophytoplankton size class (Wilkerson et al., 2006; García-Reyes et al., 2014; Hunter-Cevera et al., 2020). In this study, we analyzed twenty short-lived wind-driven events occurring when the water column was stratified (late spring, summer, and early fall) allowing the detection of clear upwelling signatures in comparison to unstratified periods. The causal effect of the physical forcing was identified using a bi-hourly time series capturing the dynamics of five phytoplankton functional groups as resolved by Automated Flow Cytometry (Dubelaar & Gerritzen, 2000; Olson et al., 2003) over two complete years. The area of interest is the French Bay of Marseille, which is considered oligotrophic in stratified periods during which it is generally affected by the regional offshore bloom occurring in winter-early spring and fall seasons (d'Ortenzio & Ribera d'Alcalà, 2009). It is dominated by pico-nanophytoplankton size classes and its hydrology is strongly influenced by North-westerlies winds generating regularly short-lived upwelling events (Bensoussan et al., 2010; Pairaud et al., 2011; Fraysse et al., 2013; Lajaunie-Salla et al., 2021; Odic et al., 2022).

2 Materials and Methods

The temperature, nutrients, and phytoplankton data were collected from September 19, 2019, to November 31, 2021, at the Sea Water Sensing Laboratory @ MIO Marseille (SSL@MM), a coastal marine station in the North-West Mediterranean Sea (43°17' N, 5°22' E). Seawater was continuously pumped at 10 meters from the coastline at a depth of 3 meters and delivered into the laboratory using a VerderFlex 40 peristaltic pump.

The seawater was coarsely pre-filtered by a PVC strainer (3 mm) and routed by polypropylene pipes that are cleaned monthly.

The temperature data were acquired every hour using an STPS sensor from the NKE-manufacturer presenting a temperature accuracy of 0.05°C. Nutrient samples were collected every four days on average and stored at -20°C until they were analyzed in a laboratory using a Technicon Autoanalyser® (SEAL Analytical) as in Tréguer and Le Corre (1975).

2.1 Phytoplankton Acquisition by Automated Pulse-shape Recording Flow Cytometry

Phytoplankton data were sampled every two hours using an Automated pulse-shape recording Flow Cytometer (Dubelaar et al., 1999; Dubelaar & Gerritzen, 2000) with the same protocol as in Marrec et al. (2018). We relied on the nomenclature proposed by Thyssen et al. (2021) (`http://vocab.nerc.ac.uk/collection/F02/current/`) and resolved five phytoplankton functional groups (PFGs): Redpicopro, Orgpicopro, Redpicoeuk, Rednano, and Orgnano, which were previously often referred to as *Prochlorococcus*, *Synechococcus*, picoeukaryotes, nanoeukaryotes, and cryptophytes, respectively. Microphytoplankton cells were collected but were not representative enough to be reported here: 75% of the samples presented less than 13 particles per milliliter. Each cell was assigned to a PFG by a Convolutional Neural Network (CNN) introduced in Fuchs et al. (2022).

2.2 Phytoplankton Biovolume, Biomass, and Growth Rate Estimations

Biovolume and biomass were estimated through empirical relationships (see Figure S1, sections 1.2 and 1.3 in Supplemental Information) following Marrec et al. (2018). The functional groups growth rate was estimated from the cell biovolumes using a size-structured population model introduced by Sosik et al. (2003) and adapted by Ribalet et al. (2015).

2.3 Wind-driven Upwelling Signatures

The occurrence and strength of each upwelling event were assessed based on the positive values of the Wind-driven Upwelling/Downwelling Index (WUDI) developed and extensively validated by Odic et al. (2022). The drop in temperature generated during an upwelling-favorable wind was evaluated as the difference between the measured water temperature and its low-pass filtered time series using a cut-off frequency of 15 days as in Rossi et al. (2014) and Odic et al. (2022). These temperature drops, or anomalies, were used to delimit three physical phases (Figure 2): (i) a pre-anomaly phase when the water temperature is stable and high, (ii) an anomaly phase when the temperature drops, stays cool for a few hours/days to then warm-up slowly, and (iii) a post-anomaly phase when the temperature has returned to a warmer and more stable state. These anomalies are particularly significant during the summer when the water column is stratified. A period was considered stratified when the filtered temperature was higher than the annual average temperature and conversely for unstratified periods as in Odic et al. (2022). Among the 54 events recorded over two years, only 20 events occurred during stratified periods and had temperature and flow cytometry data available. Besides, all successive events marked with negative seawater temperature anomalies separated by less than one day were not considered in order to have for each event a minimal relaxation time. In other words, we retain here only the significant wind-driven events happening in stratified periods that are surrounded by relatively calm periods, denoted "Stratified period Wind-induced Upwelling Event", SWUE.

The spring blooms occurring in unstratified periods were used to benchmark the biomass (and abundance) increases generated by SWUEs as the spring blooms are ex-

pected to be the most productive periods (Fraysse et al., 2013). The bloom dates were determined using the threshold method (Sapiano et al., 2012; Brody et al., 2013) and the median biomass and abundance per PFG during the bloom were used as the reference benchmark level. The biomass increase imputable to the blooms was computed using the median biomass during the week preceding the bloom as a reference value.

2.4 Rupture Detection and Response Characterization

The biological response of each PFG to the SWUE was evaluated in terms of both abundances and biomasses using a statistically-based rupture detection method presented in Truong et al. (2020). This mathematically well-founded method looked for ruptures in causal time series. It is here employed to detect potential changes in the link existing between the temperature signal and each PFG abundance or biomass. The link was here assumed to be linear (Bai & Perron, 2003) and rupture detections were performed on biomasses and abundances separately. This methodology encompasses the idea that PFGs respond to a change in their environment, and delimited the start and end of the reactions for each PFG. The response of each PFG is hence composed of three phases: a pre-reaction, a reaction, and a post-reaction phase (called the relaxation phase).

Based on the identified ruptures, four key variables per PFG were used to characterize the duration and magnitude of the biological responses as presented in Figure 2 a). The reaction delay is the time taken by a PFG to react after the rise of physical forcing, i.e. between the start of the water cooling and the beginning of the PFG automatically identified reaction. The reaction duration measures the length of the reaction phase. The reaction and relaxation magnitudes are computed as the difference in medians during the pre-reaction and reaction phases and during the reaction and relaxation phases, respectively. To capture only PFGs causal responses to sporadic upwelling events, only the PFG responses for which the reactions occurred after the beginning of the anomaly phase were considered, which was the case for most events and PFGs. The number of SWUEs taken into account for each PFG is given in Figure 3.

More material and method details are given in Supplemental Information (section 1 and Figure S2).

3 Results

3.1 Seawater Temperature and Nutrients as Markers of Sporadic Upwelling Events

The annual mean temperature over the three years was 17.8°C in 2019, 17.1°C in 2020, and 17.3°C in 2021. The associated stratified periods started on May, 8 in 2020, and May, 25 in 2021 (not available in 2019), and ended on November, 13 in 2019, October, 27 in 2020, and October, 31 in 2021. The number of significant and distinct SWUEs during the stratified periods was two in 2019, ten in 2020, and eight in 2021. The median duration anomaly phase of the SWUEs was of six days and the subsequent drops in water temperature (difference between both maximal and minimal values recorded during each SWUE) varied from 0.7°C to 9.9°C, with a median value of 4.7°C (see also Odic et al. (2022)).

Nutrient concentrations and N/P ratio were higher during unstratified periods as compared to stratified periods, except for phosphate concentration (Figure S3 in Supplemental Information; Kruskal-Wallis test, p-value $\leq$ 1.0E-7 for nitrites, nitrates, and N/P ratio, p-value ≤ 0.05 for ammonium). In stratified periods, the nitrite concentration and N/P ratios were higher and nitrate concentration lower during SWUEs than outside the SWUEs. The concentrations of phosphate and ammonium were however comparable during and outside the SWUEs. The N/P ratio was 25.15 in the unstratified pe-

riod, 17.33 during SWUEs, and 13.05 in the stratified period outside of the SWUEs. Yet, only the nitrite concentrations recorded during and outside SWUEs under stratified conditions were significantly different (Kruskal-Wallis test, p-value = 0.034). The concentrations are given in Table S1 in Supplemental Information.

3.2 Wind-induced Upwelling Events Trigger Peaks of Biomass and Abundances

All SWUEs triggered noticeable peaks of biomass for most PFGs (Figure 1 and Figure S4 in Supplemental Information). The pico-nanophytoplankton biomass was dominated in both stratification regimes by Rednano cells, followed by Orgnano, Orgpicopro, Redpicoeuk, and Redpicopro cells (Table S2 in Supplemental Information). Orgnano exceeded their median bloom biomass during one-third of the SWUEs. Similarly, more than half of the Orgpicopro and Rednano peaks went over their median bloom values. Finally, Redpicoeuk and Redpicopro biomass peak values were higher than their median bloom values in 4/5 SWUEs and all SWUEs, respectively.

In terms of abundance, the SWUEs generated peaks for most PFGs (Figure S5 in Supplemental Information). Over the whole series, the most abundant PFGs were the Orgpicopro, followed by the Redpicopro, Redpicoeuk, Rednano, and Orgnano cells (Table S3 in Supplemental Information). Near the half of Orgnano and Orgpicopro SWUE abundance peaks exceeded their median bloom abundances. Besides, more than 4/5 of SWUEs saw Rednano, Redpicoeuk and Redpicopro abundances go higher than their respective median abundances during the spring bloom.

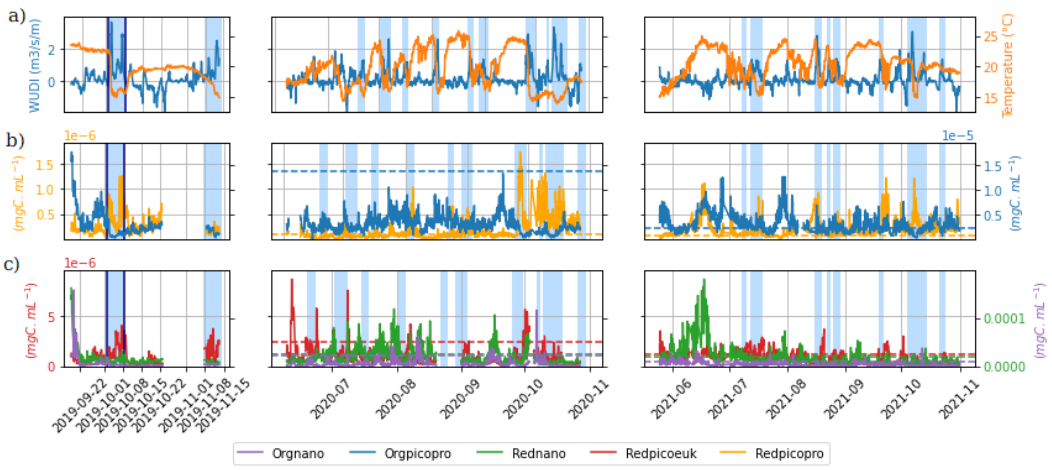

Figure 1. Time series of (a) Wind-driven Upwelling/Downwelling Index (WUDI, $m^3.s^{-1}m^{-1}$) and temperature (C°) as well as (b, c) phytoplankton biomasses ($\mu gC.mL^{-1}$) monitored at the SSL@MM coastal station. The blue rectangles correspond to the 20 studied SWUEs. The event shown in Figure 2 is bounded by a dark blue box. The horizontal dashed colored lines correspond to the median biomasses observed during the spring bloom (except for 2019, not available) for each PFG (according to the color code).

3.3 Characterization of the Phytoplankton Response: A Single Event Illustration

The typical effect of wind-induced upwellings on temperature and pico-nanophytoplankton biomass is illustrated in Figure 2, showing differentiated responses among the PFGs. This

event was fueled by three periods of intense wind forcings, or intensification periods, that generated an abrupt drop in temperature (-7.6°C) followed by the maintenance of cold waters for six days. As shown in Figure S6 in Supplemental Information, during these three sub-events, the N/P ratio rose after each wind intensification with a short delay, especially after the third one that multiplied the nitrates, nitrites, and phosphates concentration by a factor of 19, 5, and 5, respectively.

The biomass reactions of the Redpicopro, Orgpicopro, and Orgnano groups to this SWUE were quasi-instantaneous while they appeared after a short delay for the Redpicoeuk and Rednano cells (∼3 days). The biomass reaction magnitude was +42.7% for the Rednano, +123.7% for the Orgnano, +178.7% for the Redpicoeuk, +377.3% for the Redpicopro, and -82.1% for the Orgpicopro. Biomass levels decreased in the relaxation phase for all PFGs except the Orgnano.
The estimated hourly growth rates (Figure S7 in Supplemental Information) varied inversely with respect to the biomass (Figure 2) and the abundance (data not shown): when the PFG was high in biomass, its growth rate was estimated to be low and conversely.

3.4 Detailed Characterization of the Phytoplankton Response

The PFG abundances showed reaction delays ranging between 24h and 36h in median (Figure 3a). The reaction duration of the PFGs lasted between three and four days in median, with a lower Inter-Quartile Range (IQR)/median ratio than the reaction delay (Figure 3e). Concerning the reaction magnitude, the Orgnano and Orgpicopro abundances decreased while the other PFGs generally saw their abundances rising (Figure 3c). The Redpicopro and Redpicoeuk presented the largest increases in abundance. Their large IQRs were explained by some intense positive reactions for the majority of the SWUEs while only five presented moderately negative reactions for both groups. The abundance levels in the relaxation period decreased for all PFGs with median variations ranging from -28.96% to -52.85% (Figure 3g).

In terms of biomass, the Orgpicopro reacted in less than one day, the Orgnano and Redpicopro in less than two days, and Rednano and Redpicoeuk median reaction delay was three days (Figure 3b). The majority of reaction durations lasted between two and five days (Figure 3f). The signs of the reactions remained the same as for the abundance, except for the Orgnano that experienced a positive biomass reaction (Figure 3d). In the relaxation periods, the biomass levels decreased for all PFGs (-27.58% to -61.90% in median). However, positive relaxation magnitudes were observed in five SWUEs both for Orgpicopro and Rednano, explaining higher variance than for other PFGs (Figure 3h).

The estimated growth rates of the PFGs tended to slow down during the reaction phase and then increase during the relaxation phase (Figure S8 in Supplemental Information), except for the Orgpicopro. This pattern was however significant for Redpicoeuk cells only (Kruskal-Wallis test, p-value ≤ 0.01).

4 Discussion

The Bay of Marseille located in the NW Mediterranean upwelling system is a natural laboratory to explore the impact of wind-driven coastal processes on oligotrophic communities because of the unique intensities and short duration of upwelling events (Odic et al., 2022). During the stratified periods, the SWUEs had a clear signature on the seawater surface temperature. The expected signature on nutrient enrichment was less significant, probably due to the littoral conditions, the delay needed for upwelled nutrients to reach the surface sampling point, but also largely to the low and irregular nutrient sampling rates (see Figure S3 in Supplemental Information).

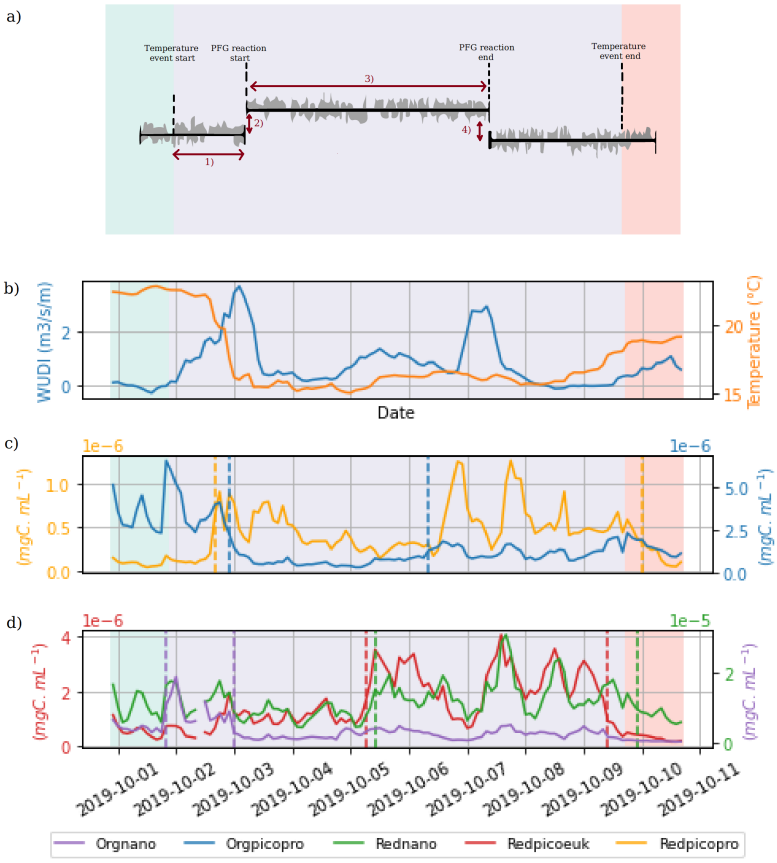

Figure 2. Illustrative view of a typical SWUE (highlighted by a dark blue box in Figure 1). a) Characterisation of the biological response to an SWUE. The grey-shaded time series represents a schematic PFG time series and the background shading corresponds to the temperature anomaly phases defining the physical event: pre-anomaly (green), anomaly (violet), and post-anomaly phase (red). The characterization is performed using four attributes: (1) the reaction delay, (2) the reaction magnitude, (3) the reaction duration, (4) and the relaxation magnitude. b) Variation of the WUDI ($m^3.s^{-1}m^{-1}$, blue line) and the temperature (°C, orange line) , c) Biomass ($mgC.mL^{-1}$) of Redpicopro and Orgpicopro d) Biomass ($mgC.mL^{-1}$) of Redpicoeuk, Rednano, and Orgnano. The vertical dashed lines represent the ruptures automatically detected by the statistical method for each PFG, according to the color code.

As mentioned in García-Reyes et al. (2014), Rossi et al. (2014), and Armbrecht et al. (2014), the physically-driven temperature drops and nutrient enrichments are key indicators to characterize the impact of SWUEs over the phytoplankton community. Using a statistical rupture detection method, the causal effects of the environmental shifts over the pico-nanophytoplankton functional groups were assessed, capturing more than simple correlations and evidencing differentiated response patterns.

The phytoplankton functional groups reacted to the SWUEs in one to five days, a delay consistent with several studies evidencing phytoplankton biomass peaks two to five days after nutrient enrichment (Edwards et al., 2005; Hauss et al., 2012; Teixeira et al., 2018). The reaction durations lasted between two and five days and were positive for all PFG abundances except for the Orgnano and Orgpicopro cells and for all PFG biomasses except for the Orgpicopro cells. The comparison with previous studies is com-

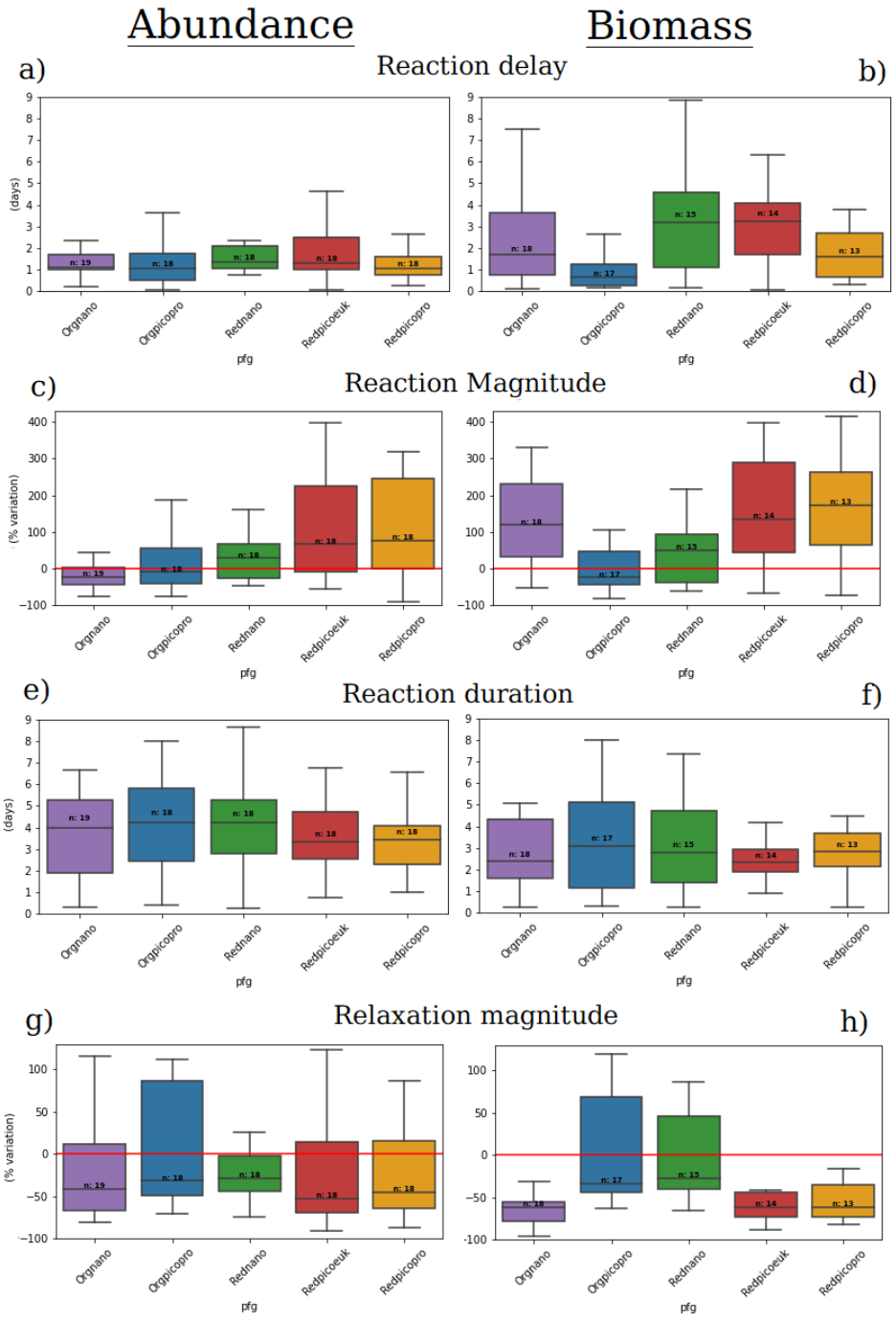

Figure 3. Boxplots of the reaction delay (a and b), the reaction magnitude (c and d), the reaction duration (e and f) and the relaxation magnitude (g and h) in terms of abundance and biomass, respectively, for five different PFGs. The horizontal red lines represent a variation of 0%. n denotes the number of SWUE for each PFG on which the boxplot has been constructed.

plicated by the different phytoplankton nomenclatures used. For instance, the increase in cyanobacteria abundance shown by Martin-Platero et al. (2018) is difficult to match with either Orgpicopro decreases or Redpicopro increases in abundance. Yet, the joint

Redpicopro abundance positive reaction and increase in N/P ratio during the event is consistent with Martiny et al. (2016). Similarly, the co-occurrence of strong biological and N/P variability is in accordance with (Martz et al., 2014). The negative sign of Orgnano reaction could be compared to the curbing abundance of cluster C5 identified in Dugenne et al. (2014) after a wind event. Similarly, Thyssen et al. (2008) have shown that two groups that presented similar red fluorescence/yellow fluorescence profiles as the Orgpicopro and Orgnano groups reacted differently than the other functional groups to the SWUEs.

After the reaction, the PFGs presented mostly negative relaxation patterns except for Orgpicopro and Orgnano during some SWUEs. As presented in Figure S9 in Supplemental Information, there seems to exist an inverse relationship between these two phases for most PFG abundances and biomasses: the more positive the reaction was, the more negative the relaxation will be for a given PFG. This can be interpreted as environmental forces pushing back to the steady state. These forces remain however to be identified and could be of various nature: nutrient depletion (Wilkerson et al., 2006), competition between functional groups (Martin-Platero et al., 2018), viral lysis or predation (Sun et al., 2007; Coello-Camba et al., 2020). Following Hunter-Cevera et al. (2014), the effect of these forces can be estimated using the model loss, i.e. the difference between the observed PFG population growth rates and their estimations by the size-structured model. The authors showed that the more correlated the loss is to the growth rate, the more likely these losses are caused by biological factors. As made visible in Figure S10 in Supplemental Information, only the Rednano and Orgnano losses were significantly but weakly correlated ($r \leq 0.31$) with their growth rates in the relaxation phase. These low or non-significant correlations between growth rates and PFG losses seem to indicate that physical forces, such as water masses mixing or water column re-stratification, as well as biogeochemical hindrances (e.g. nutrient depletion or co-limitation) are dominant during this phase as compared with grazing and viral lysis.

The PFG responses have been characterized thanks to a fine temporal and functional-level resolution. As evoked in Martin-Platero et al. (2018), the chosen taxonomic level (taxa, genera, etc.) along with the temporal frequency have a strong impact on the response patterns observed. In their studies, Martin-Platero et al. (2018) have used Operational taxonomic units (OTUs) based on rRNA sequences similarity, while Martiny et al. (2016) relied on functional groups close to the ones of this study obtained using diagnostic pigments. We used automated pulse-shape recording flow cytometry to obtain an infra-day resolution over a long period and a resolution up to the cytometric functional group. Each functional group contains several ecotypes which could affect the estimated growth rates (Hunter-Cevera et al., 2014) and add uncertainty to the size-structured model. The effect of complete PFG population replacements that could occur during extremely strong SWUEs may additionally impact the presented estimations. This is also the case of the independence between predator behaviors and the phytoplankton cell sizes assumed by the model that could not be tested here. As a result, the estimated growth rates were principally used to give context to the underlying phenomena and to emphasize the fast and remarkable impacts of SWUE on phytoplankton dynamics. Future research could hence use the introduced high-frequency methodology to derive the proper impact of SWUE on phytoplankton primary production.

Similarly, while the temporal aspects of such tight biophysical coupled mechanisms are well-resolved by our sampling strategy and numerical approach, the present study did not offer a comprehensive view of the spatial variability at stake. When coupling physics with biology, the observed biological response of the PFGs could dramatically vary depending on whether the water masses originated for example from areas near the Deep Chlorophyll Maximum, the nitracline, or the phosphacline. The phytoplankton biomass spatial dynamics, approached by chlorophyll-a concentration, have been extensively tracked by satellite (Wu et al., 2008; d'Ortenzio & Ribera d'Alcalà, 2009; Mayot et al., 2016; Lehahn

et al., 2017; El Hourany et al., 2019). However, the satellites typically have issues resolving coastal areas and submesoscale patterns, focus on surface waters, have lower temporal resolutions (e.g. daily for sea surface temperature, weekly for clear chlorophyll-a maps) and hence could not properly resolve the phytoplankton nycthemeral cycles.

In this respect, multi-year high-frequency in situ measurements, such as the ones performed at the SSL@MM coastal laboratory, could bring crucial missing pieces of information. It could for instance be complementary to the work of Alvain et al. (2008) that matched chlorophyll-a anomalies resolved by satellite with phytoplankton community structures collected in situ. Other methods such as autonomous vehicle fleets (Jaffe et al., 2017), coastal radars (HFRs) (Cianelli et al., 2017), or 3D models coupling physics and biogeochemistry (Fraysse et al., 2013) could be used jointly with the SSL@MM data to gain further insights about spatial dynamics and help guide future modeling efforts.

In summary, the SWUEs have generated significant abundance and biomass responses from the pico-nanophytoplankton community. From our data, the biggest daily biomass increase due to a single wind-induced upwelling represented 97.6% of the daily biomass increase imputable to the spring bloom. The consistent time scales and magnitudes of biological responses reported here for sporadic wind-induced events using an innovative sampling strategy and an advanced statistical methodology could provide new insights on how to observe, and perhaps model, the impact of other submesoscale events on phytoplankton communities.

Acknowledgments

The authors are grateful to Cytobuoy b.v. for the personalized software developments performed on the CytoClus4© software features. At the SSL@MM station, the data could not have been collected without the support of Michel Durand, the MIO Service Atmosphere Mer (Deny Malengros and Fabrice Garcia), and UMS OSU Pytheas (Christian Marshal and Dorian Guillemain) that maintain the pumping inlet. Additional support for the SSL@MM was provided by Aix Marseille Université, MIO, and OSU PYTHEAS. The authors are also very thankful to Ivane Pairaud and the team exploiting the MESURHO buoy for the PAR data, and to the MIO-PACEM platform for the nutrients analysis. Funding for R.F.'s Ph.D. thesis was provided by the Ministry of Higher Education, Research, and Innovation. The project leading to this publication has received funding from the ERDF under project 1166-39417. The project leading to this publication has received funding from the Excellence Initiative of Aix-Marseille University - A*MIDEX, a French "Investissements d'Avenir" program.

Open Research

The code and data to reproduce the presented results of the paper are available at `https://github.com/RobeeF/PhytoUpwellingPaper`.
The associated DOI is `https://doi.org/10.5281/zenodo.6626707`

References

Alvain, S., Moulin, C., Dandonneau, Y., & Loisel, H. (2008). Seasonal distribution and succession of dominant phytoplankton groups in the global ocean: A satellite view. *Global Biogeochemical Cycles*, *22*(3).

Antoine, D., Morel, A., & André, J.-M. (1995). Algal pigment distribution and primary production in the eastern mediterranean as derived from coastal zone color scanner observations. *Journal of Geophysical Research: Oceans*, *100*(C8), 16193–16209.

Armbrecht, L. H., Roughan, M., Rossi, V., Schaeffer, A., Davies, P. L., Waite, A. M., & Armand, L. K. (2014). Phytoplankton composition under contrast-

ing oceanographic conditions: Upwelling and downwelling (eastern australia). *Continental Shelf Research*, *75*, 54–67.

Bai, J., & Perron, P. (2003). Critical values for multiple structural change tests. *The Econometrics Journal*, *6*(1), 72–78.

Bakun, A., & Agostini, V. N. (2001). Seasonal patterns of wind-induced upwelling/downwelling in the mediterranean sea. *Scientia Marina*, *65*(3), 243–257.

Bauer, J. E., Cai, W.-J., Raymond, P. A., Bianchi, T. S., Hopkinson, C. S., & Regnier, P. A. (2013). The changing carbon cycle of the coastal ocean. *Nature*, *504*(7478), 61–70.

Bensoussan, N., Romano, J.-C., Harmelin, J.-G., & Garrabou, J. (2010). High resolution characterization of northwest mediterranean coastal waters thermal regimes: to better understand responses of benthic communities to climate change. *Estuarine, Coastal and Shelf Science*, *87*(3), 431–441.

Bolaños, L. M., Karp-Boss, L., Choi, C. J., Worden, A. Z., Graff, J. R., Haëntjens, N., ... others (2020). Small phytoplankton dominate western north atlantic biomass. *The ISME journal*, *14*(7), 1663–1674.

Borges, A. V., Delille, B., & Frankignoulle, M. (2005). Budgeting sinks and sources of co2 in the coastal ocean: Diversity of ecosystems counts. *Geophysical research letters*, *32*(14).

Bosc, E., Bricaud, A., & Antoine, D. (2004). Seasonal and interannual variability in algal biomass and primary production in the mediterranean sea, as derived from 4 years of seawifs observations. *Global Biogeochemical Cycles*, *18*(1).

Brody, S. R., Lozier, M. S., & Dunne, J. P. (2013). A comparison of methods to determine phytoplankton bloom initiation. *Journal of Geophysical Research: Oceans*, *118*(5), 2345–2357.

Cianelli, D., D'Alelio, D., Uttieri, M., Sarno, D., Zingone, A., Zambianchi, E., & d'Alcalà, M. R. (2017). Disentangling physical and biological drivers of phytoplankton dynamics in a coastal system. *Scientific reports*, *7*(1), 1–15.

Coello-Camba, A., Diaz-Rua, R., Duarte, C. M., Irigoien, X., Pearman, J. K., Alam, I. S., & Agusti, S. (2020). Picocyanobacteria community and cyanophage infection responses to nutrient enrichment in a mesocosms experiment in oligotrophic waters. *Frontiers in Microbiology*, *11*, 1153. Retrieved from `https://www.frontiersin.org/article/10.3389/fmicb.2020.01153` doi: 10.3389/fmicb.2020.01153

d'Ortenzio, F., & Ribera d'Alcalà, M. (2009). On the trophic regimes of the mediterranean sea: a satellite analysis. *Biogeosciences*, *6*(2), 139–148.

Dubelaar, G. B., & Gerritzen, P. L. (2000). Cytobuoy: a step forward towards using flow cytometry in operational oceanography. *Scientia Marina*, *64*(2), 255–265.

Dubelaar, G. B., Gerritzen, P. L., Beeker, A. E., Jonker, R. R., & Tangen, K. (1999). Design and first results of cytobuoy: A wireless flow cytometer for in situ analysis of marine and fresh waters. *Cytometry: The Journal of the International Society for Analytical Cytology*, *37*(4), 247–254.

Dugenne, M., Thyssen, M., Nerini, D., Mante, C., Poggiale, J.-C., Garcia, N., ... Grégori, G. J. (2014). Consequence of a sudden wind event on the dynamics of a coastal phytoplankton community: an insight into specific population growth rates using a single cell high frequency approach. *Frontiers in microbiology*, *5*, 485.

Edwards, V., Icely, J., Newton, A., & Webster, R. (2005). The yield of chlorophyll from nitrogen: a comparison between the shallow ria formosa lagoon and the deep oceanic conditions at sagres along the southern coast of portugal. *Estuarine, Coastal and Shelf Science*, *62*(3), 391–403.

El Hourany, R., Abboud-abi Saab, M., Faour, G., Mejia, C., Crépon, M., & Thiria, S. (2019). Phytoplankton diversity in the mediterranean sea from satellite data using self-organizing maps. *Journal of Geophysical Research: Oceans*, *124*(8),

5827–5843.

Fraysse, M., Pinazo, C., Faure, V. M., Fuchs, R., Lazzari, P., Raimbault, P., & Pairaud, I. (2013). Development of a 3d coupled physical-biogeochemical model for the marseille coastal area (nw mediterranean sea): what complexity is required in the coastal zone? *PloS one*, *8*(12), e80012.

Fuchs, R., Thyssen, M., Creach, V., Dugenne, M., Izard, L., Latimier, M., ... Pommeret, D. (2022). Automatic recognition of flow cytometric phytoplankton functional groups using convolutional neural networks. *Limnology and Oceanography: Methods*. doi: https://doi.org/10.1002/lom3.10493

García-Reyes, M., Largier, J. L., & Sydeman, W. J. (2014). Synoptic-scale upwelling indices and predictions of phyto-and zooplankton populations. *Progress in Oceanography*, *120*, 177–188.

Gattuso, J., Frankignoulle, M., & Wollast, R. (1998). Carbon and carbonate metabolism in coastal aquatic ecosystems. *Annual Review of Ecology, Evolution, and Systematics*, *29*, 405-434.

Grob, C., Ulloa, O., Claustre, H., Huot, Y., Alarcon, G., & Marie, D. (2007). Contribution of picoplankton to the total particulate organic carbon concentration in the eastern south pacific. *Biogeosciences*, *4*(5), 837–852.

Hauss, H., Franz, J. M., & Sommer, U. (2012). Changes in n: P stoichiometry influence taxonomic composition and nutritional quality of phytoplankton in the peruvian upwelling. *Journal of sea Research*, *73*, 74–85.

Hunter-Cevera, K. R., Neubert, M. G., Olson, R. J., Shalapyonok, A., Solow, A. R., & Sosik, H. M. (2020). Seasons of syn. *Limnology and oceanography*, *65*(5), 1085–1102.

Hunter-Cevera, K. R., Neubert, M. G., Solow, A. R., Olson, R. J., Shalapyonok, A., & Sosik, H. M. (2014). Diel size distributions reveal seasonal growth dynamics of a coastal phytoplankter. *Proceedings of the National Academy of Sciences*, *111*(27), 9852–9857.

Jaffe, J. S., Franks, P. J., Roberts, P. L., Mirza, D., Schurgers, C., Kastner, R., & Boch, A. (2017). A swarm of autonomous miniature underwater robot drifters for exploring submesoscale ocean dynamics. *Nature communications*, *8*(1), 1–8.

Lajaunie-Salla, K., Diaz, F., Wimart-Rousseau, C., Wagener, T., Lefèvre, D., Yohia, C., ... Pinazo, C. (2021). Implementation and assessment of a carbonate system model (eco3m-carbox v1. 1) in a highly dynamic mediterranean coastal site (bay of marseille, france). *Geoscientific Model Development*, *14*(1), 295–321.

Lehahn, Y., Koren, I., Sharoni, S., d'Ovidio, F., Vardi, A., & Boss, E. (2017). Dispersion/dilution enhances phytoplankton blooms in low-nutrient waters. *Nature Communications*, *8*(1), 1–8.

Lévy, M., Ferrari, R., Franks, P. J., Martin, A. P., & Rivière, P. (2012). Bringing physics to life at the submesoscale. *Geophysical Research Letters*, *39*(14).

Li, W. (1995). Composition of ultraphytoplankton in the central north atlantic. *Marine Ecology Progress Series*, *122*, 1–8.

Lomas, M. W., & Moran, S. B. (2011). Evidence for aggregation and export of cyanobacteria and nano-eukaryotes from the sargasso sea euphotic zone. *Biogeosciences*, *8*(1), 203–216.

Lomas, M. W., Roberts, N., Lipschultz, F., Krause, J., Nelson, D., & Bates, N. (2009). Biogeochemical responses to late-winter storms in the sargasso sea. iv. rapid succession of major phytoplankton groups. *Deep Sea Research Part I: Oceanographic Research Papers*, *56*(6), 892–908.

Marrec, P., Grégori, G., Doglioli, A. M., Dugenne, M., Della Penna, A., Bhairy, N., ... Thyssen, M. (2018). Coupling physics and biogeochemistry thanks to high-resolution observations of the phytoplankton community structure in the northwestern mediterranean sea. *Biogeosciences*, *15*(5), 1579–1606. Re-

trieved from https://bg.copernicus.org/articles/15/1579/2018/ doi: 10.5194/bg-15-1579-2018

Martin-Platero, A. M., Cleary, B., Kauffman, K., Preheim, S. P., McGillicuddy, D. J., Alm, E. J., & Polz, M. F. (2018). High resolution time series reveals cohesive but short-lived communities in coastal plankton. *Nature communications*, *9*(1), 1–11.

Martiny, A. C., Talarmin, A., Mouginot, C., Lee, J. A., Huang, J. S., Gellene, A. G., & Caron, D. A. (2016). Biogeochemical interactions control a temporal succession in the elemental composition of marine communities. *Limnology and Oceanography*, *61*(2), 531–542.

Martz, T., Send, U., Ohman, M. D., Takeshita, Y., Bresnahan, P., Kim, H.-J., & Nam, S. (2014). Dynamic variability of biogeochemical ratios in the southern california current system. *Geophysical Research Letters*, *41*(7), 2496–2501.

Mayot, N., d'Ortenzio, F., Ribera d'Alcalà, M., Lavigne, H., & Claustre, H. (2016). Interannual variability of the mediterranean trophic regimes from ocean color satellites. *Biogeosciences*, *13*(6), 1901–1917.

Millot, C. (1979). Wind induced upwellings in the gulf of lions. *Oceanologica Acta*, *2*(3), 261–274.

Morel, A., & André, J.-M. (1991). Pigment distribution and primary production in the western mediterranean as derived and modeled from coastal zone color scanner observations. *Journal of Geophysical Research: Oceans*, *96*(C7), 12685–12698.

Odic, R., Bensoussan, N., Pinazo, C., Taupier-Letage, I., & Rossi, V. (2022). Sporadic wind-driven upwelling/downwelling and associated cooling/warming along northwestern mediterranean coastlines. *Continental Shelf Research (under final revision)*.

Olson, R. J., Shalapyonok, A., & Sosik, H. M. (2003). An automated submersible flow cytometer for analyzing pico-and nanophytoplankton: Flowcytobot. *Deep Sea Research Part I: Oceanographic Research Papers*, *50*(2), 301–315.

Pairaud, I., Gatti, J., Bensoussan, N., Verney, R., & Garreau, P. (2011). Hydrology and circulation in a coastal area off marseille: Validation of a nested 3d model with observations. *Journal of marine systems*, *88*(1), 20–33.

Palma, E. D., & Matano, R. P. (2009). Disentangling the upwelling mechanisms of the south brazil bight. *Continental Shelf Research*, *29*(11-12), 1525–1534.

Ribalet, F., Swalwell, J., Clayton, S., Jiménez, V., Sudek, S., Lin, Y., ... Armbrust, E. V. (2015). Light-driven synchrony of prochlorococcus growth and mortality in the subtropical pacific gyre. *Proceedings of the National Academy of Sciences*, *112*(26), 8008–8012.

Richardson, T. L., & Jackson, G. A. (2007). Small phytoplankton and carbon export from the surface ocean. *Science*, *315*(5813), 838–840.

Rossi, V., Garçon, V., Tassel, J., Romagnan, J.-B., Stemmann, L., Jourdin, F., ... Morel, Y. (2013). Cross-shelf variability in the iberian peninsula upwelling system: Impact of a mesoscale filament. *Continental Shelf Research*, *59*, 97–114.

Rossi, V., Schaeffer, A., Wood, J., Galibert, G., Morris, B., Sudre, J., ... Waite, A. M. (2014). Seasonality of sporadic physical processes driving temperature and nutrient high-frequency variability in the coastal ocean off southeast australia. *Journal of Geophysical Research: Oceans*, *119*(1), 445–460.

Sapiano, M., Brown, C., Schollaert Uz, S., & Vargas, M. (2012). Establishing a global climatology of marine phytoplankton phenological characteristics. *Journal of Geophysical Research: Oceans*, *117*(C8).

Sosik, H. M., Olson, R. J., Neubert, M. G., Shalapyonok, A., & Solow, A. R. (2003). Growth rates of coastal phytoplankton from time-series measurements with a submersible flow cytometer. *Limnology and Oceanography*, *48*(5), 1756–1765.

Sun, J., Feng, Y., Zhang, Y., & Hutchins, D. (2007, 09). Fast microzooplankton grazing on fast-growing, low-biomass phytoplankton: A case study in spring in

chesapeake bay, delaware inland bays and delaware bay. *Hydrobiologia*, *589*, 127-139. doi: 10.1007/s10750-007-0730-6

Teixeira, I., Arbones, B., Froján, M., Nieto-Cid, M., Álvarez-Salgado, X. A., Castro, C. G., ... Figueiras, F. (2018). Response of phytoplankton to enhanced atmospheric and riverine nutrient inputs in a coastal upwelling embayment. *Estuarine, Coastal and Shelf Science*, *210*, 132–141.

Thyssen, M., Fuchs, R., Créach, V., Artigas, L. F., Grégori, G., Marrec, P., ... others (2021). Standard vocabulary, consensual functional groups and automated classification for phytoplankton high throughput datasets using automated flow cytometry. In *Aslo 2021.*

Thyssen, M., Mathieu, D., Garcia, N., & Denis, M. (2008). Short-term variation of phytoplankton assemblages in mediterranean coastal waters recorded with an automated submerged flow cytometer. *Journal of Plankton Research*, *30*(9), 1027–1040.

Tréguer, P., & Le Corre, P. (1975). Manuel d'analyse des sels nutritifs dans l'eau de mer (utilisation de l'autoanalyseur ii technicon), 110, lab. d'océanogr. *Chim., Univ. de Bretagne Occident., Brest, France*.

Truong, C., Oudre, L., & Vayatis, N. (2020). Selective review of offline change point detection methods. *Signal Processing*, *167*, 107299.

Wilkerson, F. P., Lassiter, A. M., Dugdale, R. C., Marchi, A., & Hogue, V. E. (2006). The phytoplankton bloom response to wind events and upwelled nutrients during the coop west study. *Deep Sea Research Part II: Topical Studies in Oceanography*, *53*(25-26), 3023–3048.

Wimart-Rousseau, C., Lajaunie-Salla, K., Marrec, P., Wagener, T., Raimbault, P., Lagadec, V., ... others (2020). Temporal variability of the carbonate system and air-sea co2 exchanges in a mediterranean human-impacted coastal site. *Estuarine, Coastal and Shelf Science*, *236*, 106641.

Wu, Y., Platt, T., Tang, C. C., Sathyendranath, S., Devred, E., & Gu, S. (2008). A summer phytoplankton bloom triggered by high wind events in the labrador sea, july 2006. *Geophysical Research Letters*, *35*(10).